Lasers in Manufacturing Conference 2017

Recent advances in the multiphysical simulation of laser assisted manufacturing processes

Rodrigo Gómez Vázquez[a,*], Andreas Otto[a], Jaka Peternel[b]

[a] *Vienna University of Technology, Getreidemarkt 9, Vienna 1060, Austria*
[b] *University of Ljubljana, Kongresni trg 12, Ljubljana 1000, Slovenia*

Abstract

The industrial implementation of laser assisted processing technologies is nowadays well-established due to the unique combination of accuracy, productivity and adaptability that laser sources permit. As laser assisted techniques allow for precisely controlling the thermal heat input it is possible e.g. to produce high-end components with a minimum influence on the functional characteristics. On the other hand, finding optimal process parameters is often a difficult task which involves the use of experimental methods that not always provide enough relevant process information. In this regard numerical simulations can help to fill this gap with the use of multiphysical models.
In this paper we present both recent achievements as well as current ongoing work lines of a multiphysical model designed to accomplish the simulation of laser assisted manufacturing processes. The general design of the model allows for the simulation of different kinds of laser processes such as welding, cutting or more recently even ultra-short pulse ablation [1]. The model is able to perform the simulation of the complete process, thus providing useful information such as the influence of keyhole front inclination or of surface tension on the flow of the molten material and its consequences after the solidification. New developments presented are aimed to extend the physical capabilities of the current model as well as to improve the calculation performance in massively parallel scenarios such as HPC-clusters or cloud environments.

Keywords: multiphysics; simulation; laser welding; laser cutting

* Corresponding author. Tel.:+43-1-058801-311626; fax: +43-1-058801-9-311611.
E-mail address: rodrigo.gomez.vazquez@tuwien.ac.at .

1. Introduction

The aim of this paper is to provide an overview of the recent achievements as well as the current ongoing work involving the multiphysical simulation of laser assisted processes at our research group.

1.1. Simulation model

The simulation environment used is OpenFOAM®. This software is an open source package suitable for the simulation of continuum physics on a Finite Volume approach that is used to solve systems of partial differential equations. It contains the necessary libraries for parallel calculations and though there are many solvers for general CFD-applications available, the programing syntax adopted allows for convenient implementation of more specific physical models on their top.

In our case, we started from a solver called *multiphaseInterDyMFoam*, which is designed for the simulation of turbulent incompressible isothermal multiphase segregated flows with automatic re-meshing operations. It makes use of a Volume of Fluid formulation conveniently extended to deal with an unlimited number of phases. It must be emphasized that the concept of "phase" employed here is not equivalent to "material". Thus it is possible to define different phases of a same material in a simulation, each one having its own physical properties e.g. for solid and liquid state. The concept of phase-mixture is used to average the physical properties at every mesh cell, taking into account either the volume- or the mass-fraction of the phases present in each cell (depending on the physical meaning of the property being evaluated).

Several changes aimed to enhance the capabilities of the standard solver in order to simulate laser manufacturing processes in general were accomplished. Here we will only summarize the main of them:

The propagation of the laser intensity is modelled using a differential form of the radiative transfer equation. This approach takes into account partial attenuation due to semi-transparent media such as plasma, but it is not suitable for the calculation of multiple reflections. Therefore a ray tracing method that accounts for this effect is coupled right after the 1st incidence occurs. The angle of incidence determines the reflectivity according to Fresnel equations. Instead of coupling the absorbed energy directly in the energy conservation equation we place this source term in the electron side of a two-temperature model. The energy is initially absorbed by the electrons and only then transferred to the lattice by means of a coupling function until a thermal equilibrium between electrons and lattice is reached (see details in [2]). This procedure does not alter the results of conventional laser processes such as welding or cutting and it is of crucial importance for the simulation of ultra-short pulse ablation processes. An enthalpy-based energy conservation equation allows the calculation of heat transfer, which eventually leads to a greater or lesser extent into phase changes. At least solid, liquid and vapor states shall be defined as independent phases for each material. The phases and energy available inside a certain mesh element determine the magnitude of the phase change. For melting and solidification this implementation is similar to the one presented in [3]. Unfortunately this is not possible for the case of evaporation and condensation. We apply Clausius-Clapeyron model for these phase changes, which does not only depend on the latent heat, but also on the temperature and on the local pressure. In many times we use an ideal-gas approach to calculate the properties of the vapor phases. The specific volume is temperature- as well as pressure-dependent, what means that the amount of vaporizing mass influences the local pressure and thus the phase change itself too. For this reason, these phase changes demand an additional iteration step. In order to avoid unphysically high velocities arising from the sudden expansion from condensed to gaseous state a compression model which deals with the concept of relative densities has been implemented (see details in [4]). Restriction of

solid-phases movement is imposed by introducing a suitable source term into the equation of momentum conservation and the surface tension model was modified to account for surface tangential forces instead of normal ones, which is essential to resolve thermo-capillary driven meltpool flows.

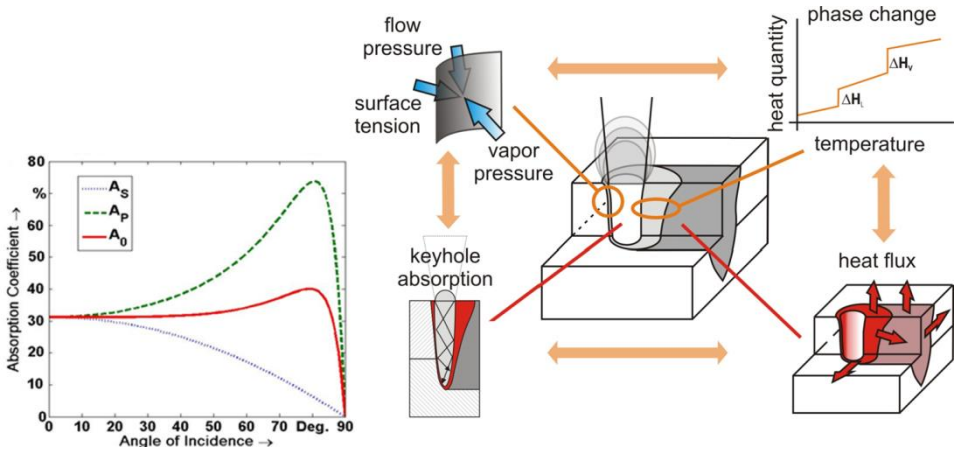

Fig. 1. Schematic summary of the simulation model.

The main conception of the simulation model consists on coupling physical laws, mostly implemented in form of differential equations, instead of simply using empirical models designed to describe specific cases. This general design is the key that makes possible the study of a wide range of conditions without substantial changes. Furthermore, the simultaneous solution of the numerous physics involved provides valuable information for the in-depth study of processes e.g. problems, causes and possible optimizing strategies.

2. Applications

In the following we will show a couple of application examples where the use of the simulation model helped to progress in the understanding of the relevant process mechanisms involved.

2.1. Ablation cutting

This study is the result of common work with the Laserinstitut Hochschule Mitweida, where the experimental work has been carried out. More details can be found in [5] (in German language). The aim of the study was to understand the dynamic mechanisms dominating the ablation process. The studied domain starts beyond the beginning of the process window for low feed rates and goes towards the upper limit. According to the experimental results three main regimes have been identified: The first one is a pure welding regime for low feed rates up to 2 m/s. There is an ablation regime for feed rates above 6 m/s. For feed rates in between those values there is a transition zone at which the process cannot be clearly classified into any of the latter ones.

Table 1. Parameters used for the study of laser ablation [5].

Workpiece material	Plate thickness	Wavelength	Power	Spot size	Feed rate
Steel 1.4301	1mm	1,06 µm	1 kW	25 µm	from 1 to 15 m/s

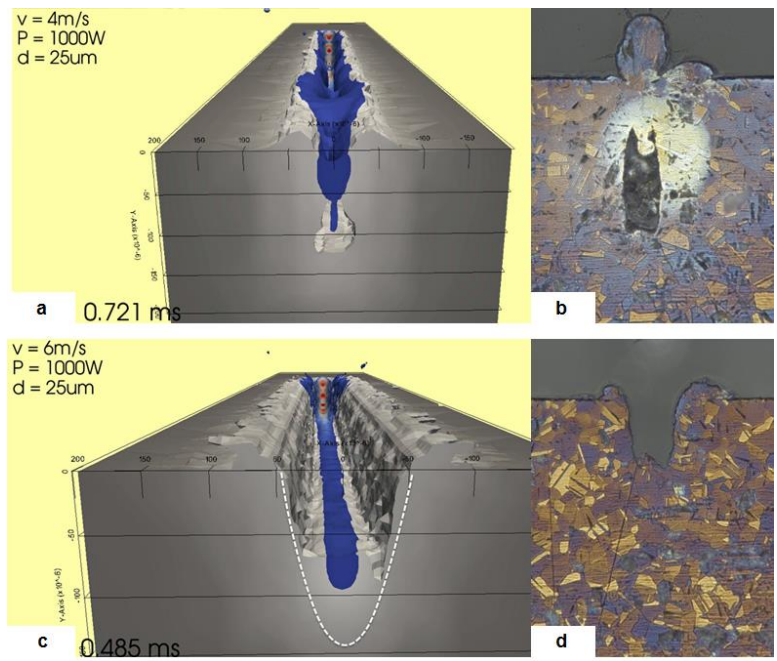

Fig. 2. (a) and (b) [5] Comparison between simulation results and experimental results at a feed rate of 4 m/s; (c) and (d) [5] Comparison between simulation results and experimental results at a feed rate of 6 m/s. The dotted line in (c) indicates the initial penetration.

Fig. 2 shows a couple of simulation results along with the corresponding experimental conditions. The first of them corresponds to the transition regime and the main characteristics are big voids that are left roofed by solidified melt bridges. The other one shows melt stream along the root which gradually fills the ablation notch as well as some burrs at the top of the flanges. The reasons for these phenomena can be well explained by a simulation-supported process analysis:

Fig. 3 depicts the evolution of the process from a keyhole welding regime taking place at 1 m/s until the ablation one at 15 m/s. In the first case there is a deep narrow keyhole where the melt accumulates at the rear due to the vaporization that is happening at the front. Part of this melt is ejected upwards at the beginning, as usual in deep penetration welding. In the second case, which also corresponds to the condition depicted in Fig. 2 (a) two different mechanisms for the melt evacuation from the absorption front can be identified. One originates at the bottom of the front and flows backwards along the notch root, therefore it will be denoted as the root stream. The other one appears laterally and propagates backwards along the flanges. This latter one will be denoted as the flange stream. The root stream is formed by the molten material which was pressed downwards due to the recoil pressure of the vaporizing material at the front. The flange stream comprises the portion of molten material which was pushed to the sides upwards due to

the combined action of the recoil pressure and drag from the escaping vapor and which did not reach enough momentum to break the surface tension and leave the kerf in form of droplet jets. The upward component of this stream depends on the inclination of the absorption front because the repulsion forces (recoil pressure or vapor drag) are perpendicular to it. Increasing the feed rate of the process the upward component of the flange stream rises, thus increasing the amount of liquid that is ejected in form of spatters. Simultaneously the root stream gets favored because the recoil pressure pushes more material down. The combined result is an enlargement of the root stream flow and a reduction of the flange stream one.

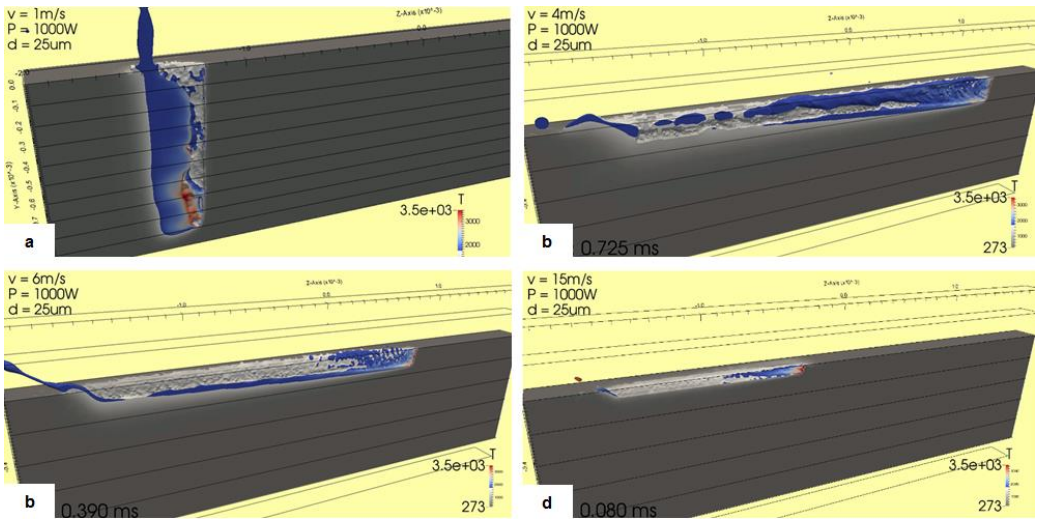

Fig. 3. Simulation results for different feed rates: (a) 1 m/s; (b) 4 m/s; (c) 6 m/s; (d) 15 m/s.

In principle, the presence of any of these streams has negative consequences for the ablation process. In the case of having an intense flange stream (Fig. 3(b)) the solidification taking place at the sides decreases the offset between flanges and the approaching streams end up bridging the gap and merging. Under the right conditions the vapor flowing backwards along the kerf can sustain these streams long enough at the upper side of the flanges until they fuse and solidify, leading into structures such as the one depicted by Fig. 2.(a) and Fig. 2(b). If the flange stream is pushed upwards more severely, the fraction of the liquid film that is not teared out at the top will leave a characteristic burr pattern. The effect of the root stream is more likely to go unnoticed, because it basically fills up the kerf from the bottom, making the original penetration hard to identify. Nevertheless, it also leaves a characteristic footprint in form of a small convex bead along the root of the notch. Fig. 2 (b) shows this re-filling mechanism as well as the original penetration depth measured in the simulations.

2.2. Study of humping phenomenon

As above mentioned, the universal design of the model becomes advantageous for its use in process analysis. In this example the goal was to understand the physical mechanisms behind the so-called humping phenomenon. Humps are characteristic drop-like shapes that appear with certain intermittence on the top of a weld bead when operating at high feed rates (see Fig. 4). They have been observed over the last 50

years and though different approaches have been suggested up to now none of them could fully explain the occurrence of this phenomenon. This work is part of a common study between the Ernst-Abe-University of Applied Science in Jena (Germany) and our group at the Technical University of Vienna (Austria). More details about this study can be found in [6]. For this analysis we chose a set of conditions that evidenced humping behavior in the experimental tests of laser micro welding. These are presented in the Table 2.

Table 2. Studied conditions for laser micro welding[6].

Workpiece material	Foil thickness	Wavelength	Power	Spot size	Feed rate
Stainless steel	100 µm	1,07 µm	400 W	25 µm and 65 µm	1.2 m/s

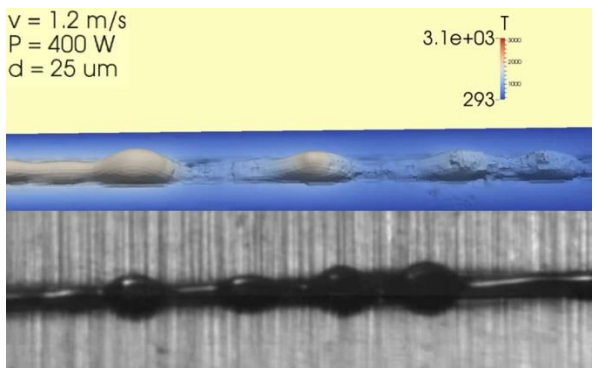

Fig. 4. Hump structures given by the simulations as well as by the experimental test with the spot size of 25µm.

Fig. 5 shows a descriptive view of the main areas involved in the process of hump formation. The most decisive one is again the absorption front, whose angle directly relates to the feed rate applied. In this zone is where the species evaporation takes place. Thus the direction of the resulting vapor flow is originally normal to the absorption front. In addition, the recoil pressure, which also acts normally to the front, forces the molten material to flow away laterally, from where it continues flowing backwards along the walls of the elongated keyhole. This is result of the high pressure induced by the vaporizing process at the front. The initial upwards component of this flow due to the combined effect of the vapor flow drag forces and of the front pressing (both perpendicular to the front) can be appreciated from the scheme given in Fig. 5. At the precise conditions leading into humping this component does not reach to release spatter ejections like in the ablation process discussed above, but is high enough to produce an upwards melt stream. Furthermore, the heat is also transported upwards along with the liquid stream, thus inducing faster solidification at the lower part of the foil. The side streams eventually create bridges analogously as in the discussed case of frustrated ablation (Fig. 3(b)). The melt solidifies starting from the bottom ant it creates a ramp-like front along which the forthcoming molten material will be conducted to flow up to the top of the foil. In addition there is an accumulation of the melt at the rear instead of a homogeneous spreading due to the effect of surface tension. These two phenomena amplify each other: on the one hand the ramped solidification front directs the melt upwards and on the other hand the upwards solidification gets more pronounced due to the heat accumulation at the top brought by the melt species. With the further advance of the solidification front the feedline of the hump finally gets constricted and the hump solidifies, leaving that characteristic

droplet-like shape. Once leaving the hump behind, the solidification ramp recovers its initial inclination and the cycle starts again. Fig.6 shows different stages of this process.

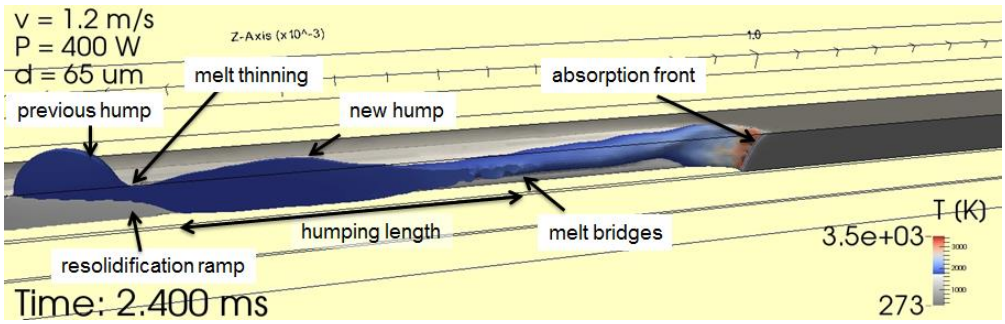

Fig. 5. Schematic view of the process showing the most relevant areas involved.

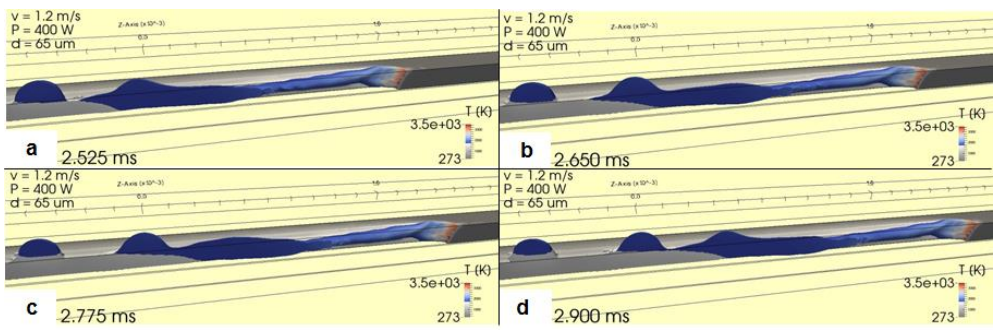

Fig. 6. Different stages of the hump formation in the course of the micro welding process.

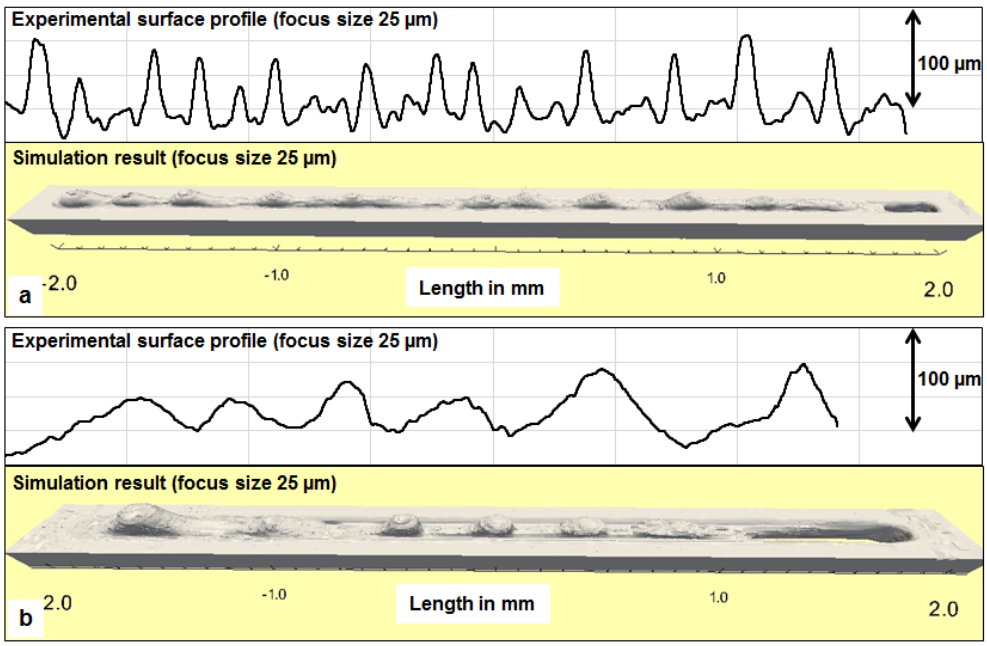

Fig. 7. Comparison between simulation results and experimental ones with the spot size of 25 µm.

In a qualitative assessment we observe that the frequency of the humps seems to be related with the distance between the solidification front and the melt bridges, what we call "humping length", as well as with the length of the elongated keyhole (see Fig. 5). The shorter these two distances are the higher hump frequency can be expected. Also in this aspect the simulation results were in good agreement with the experiments, as seen in Figure 7. In addition these distances increase when using bigger spot sizes, mainly because of the broader offset between the sides of the elongated keyhole.

3. Ongoing work

3.1. Beam propagation

As previously mentioned, the propagation of the laser beam by a means of a transport equation for the intensity has some limitations. Most notable one is the impossibility of simulating successive reflections. On the other hand, the ray tracing model used to account for these multiple reflections cannot calculate the attenuation of the beams while crossing translucent media. According to Beer Lambert law, the intensity along the propagation direction is given by following expression:

$$\frac{dI(z)}{dz} = -\mu I(z) \qquad (1)$$

being $I(z)$ the intensity along the propagation direction, z the propagation direction and μ the attenuation coefficient of the propagation medium at given wavelength. Such equation cannot be solved using common linear algebra methods, so the current implementation we have is based on the analytical solution for the one dimensional propagation:

$$I = I_0 e^{-\mu \Delta z} \tag{2}$$

where I_0 is the original intensity and Δz the propagation distance across the translucent medium. If we consider the laser radiation as a set of Lagrangian parcels, representing each a considerable amount of photons and propagating inside a surrounding medium; the energetic interaction between the "photon parcel" and the surrounding medium can be at any time represented by the one dimensional propagation equation:

$$E_{parcel} = E_{0_{parcel}} e^{-\mu \cdot c_0 \cdot \Delta t} \tag{3}$$

where $E_{0\ parcel}$ and E_{parcel} denote the energy at the emission and after a certain time Δt from the emission, respectively, and c_0 is the speed of the light inside the surrounding medium. We consider parcels of photons instead of photons mainly because of practical reasons. Apart from the fact that the evolution of a single photon is not very relevant in terms of the process scale, it would not be physically accurate to deal with energy losses in photons for a constant wavelength. One can see for example such parcels as an energy discretization method, similar as using coarser or finer meshes for the spatial domain.

Likewise as done with other pieces of the simulation model, we modified an existing library for the simulation of Lagrangian tracers in order to match our requirements. Every time step we introduce a new set of parcels from a boundary of the simulation domain (emission point). The propagation of the parcels from the emission point follows a field flow that resembles the shape of a Gaussian beam. The parcels can continuously transfer energy to the containing mesh cells according to equation 4. If there are several phases coexisting at the same cell then the attenuation coefficient is averaged. When reaching an interface, the reflection is calculated by flipping the propagation direction relative to the surface normal vector and the parcel continues its travel with a straight-linear propagation. The solution of Fresnel equations gives the energy remaining in the parcel after being reflected. In addition we create a new parcel at the same position, whose energy is the difference between the incoming and the reflected one in order to represent the fraction of refracted light. Such particle propagates with a straight-linear movement too, but along a direction that is calculated according to Snell´s refraction law, where the case of total reflection is also considered. In the course of a usual simulation one cannot see the parcels. Because of their high propagation velocity they leave the domain in a much shorter extend than a typical time step length (although this is not necessarily true in case of simulating femtosecond pulses). The movement of these parcels can only be seen if artificially lowering their propagation velocity for debugging purposes like shown in Fig. 8. Lastly, the particles are removed when their energy goes down under a certain threshold value in order to speed up the calculation.

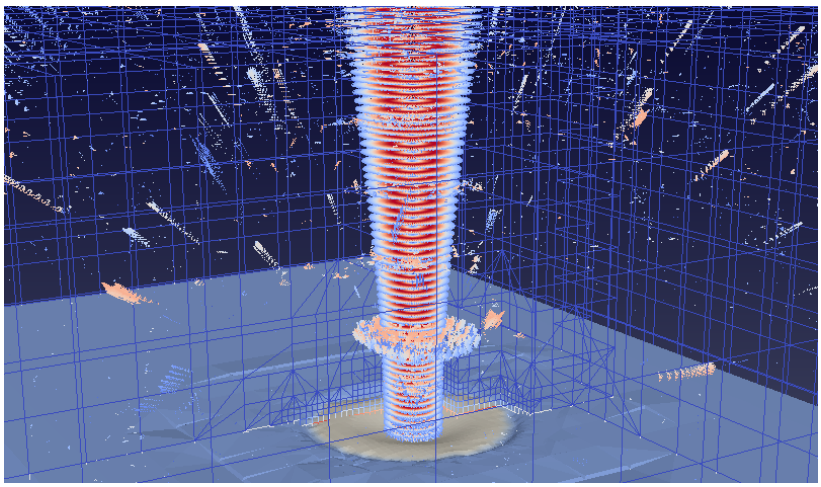

Fig. 8. Actual photon parcels being reflected on the surface of a meltpool in a low propagation speed test. They cannot be seen during conventional simulations. Unphysical reflections in the surrounding medium over the meltpool are due to numerical diffusion of the liquid phase.

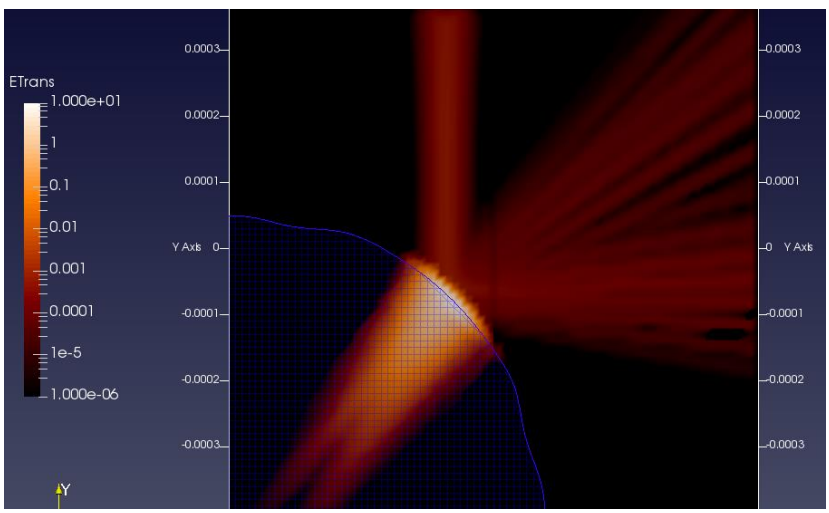

Fig. 9. Energy source terms transferred to the continuum domain in an exemplary simulation of two semi-transparent media. Normalized values in logarithmic scale. The incident beam enters into the domain from the top. Once reaching the interface with a less transmissive medium it experiences reflection as well as refraction.

The advantage of this technique is that there is no actual distinction in the simulation of opaque, transparent or translucent phases. The final distribution of energy in the domain depends only on the local extinction coefficients (see Fig. 9).

3.2. Performance in parallel

One usual requirement for the process simulations is a reasonable calculation time, especially when the results are needed to support decisions within an industrial scope. On the other hand, the solution of multiphysical problems inherently involves a huge calculation demand. For this reason is important to work with a code that allows high-scale parallel computing. In general, OpenFOAM software allows excellent performance scaling in parallel environments. The performance rises almost linearly with the number of cores up to reference levels of around 10-20 thousand cells per core. While developing our solver on the top of it we tried to avoid non-parallelizable code as much as possible and thanks to that we are able to reach similar parallel performance marks in our benchmark tests as shown in Fig. 10.

One of the key features that allow whole process scale simulations is the use of Adaptive Mesh Refinement (AMR) techniques. These are already within the simulation software and allow refining regions basing on pre-defined parameters. For instance, while having a coarse background mesh for the workpiece and the surrounding medium, one may want to have a higher resolution at the meltpool in order to get a good description of the flow patterns and a higher one of the angle dependent absorption at the exposed surface (see Fig. 11 (a)). The fact that these regions are in continuous evolution implies that so does the mesh refinement. For single core simulations this approach allows the most efficient calculation. However, in parallel scenarios it is not necessarily the case.

When preparing a simulation in parallel the simulation domain gets divided in a more simple or complex geometrical way and each parallel process is in charge of the simulation of its own part of the original domain. In the course of the simulation and due to the continuous changes in the regions that must be re-meshed, some of the processes will end up having higher amount of cells than others. That leads to an unbalanced calculation where the bottleneck is set by the process with the highest load (typically the amount of cells). Other approaches like setting a pre-established refined mesh where the regions of interest are supposed to be is often a risky assumption and also inefficient, because it leads to an overall higher amount of cells. On the other hand the use of highly parallelized environments such as cloud computing services or dedicated HPC-cluster centers involves an economical investment. Therefore it is of main importance to use these resources as efficient as possible and that requires a more sophisticated calculation approach.

With this aim we recently coupled our model with a tool that allows for load balancing during the runtime. If the load imbalance among processes during the simulation exceeds at any time a predefined threshold value a redistribution of the simulation domain among the processes takes place in order to ensure a continuously quassi-balanced run and therefore an efficient use of the available hardware resources. Fig. 11 (b) shows the performance comparison of a benchmark test where the same case was simulated using 16 cores on a single node with three different approaches: a constant pre-refined grid of about 6.5 millions of elements in the regions where high resolution demand was expected (different from the one above mentioned); two grids with automatic AMR, one with invariant process distribution and the other one with automatic load balancing, both ending up with about 2.6 millions of elements.

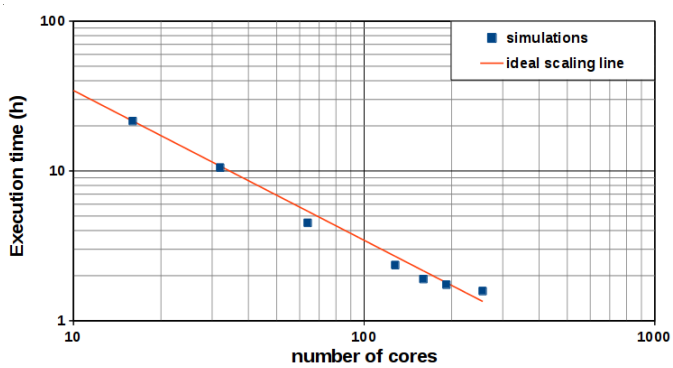

Fig. 10. Simulation performance in parallel for a benchmark case with a fixed grid of about 4 million of elements. The red line indicates the ideal trend where the simulation time decreases linearly with the number of cores used. The beginning of the stagnation area shows up at a level of exactly 20 thousand cells per core when using 192 cores.

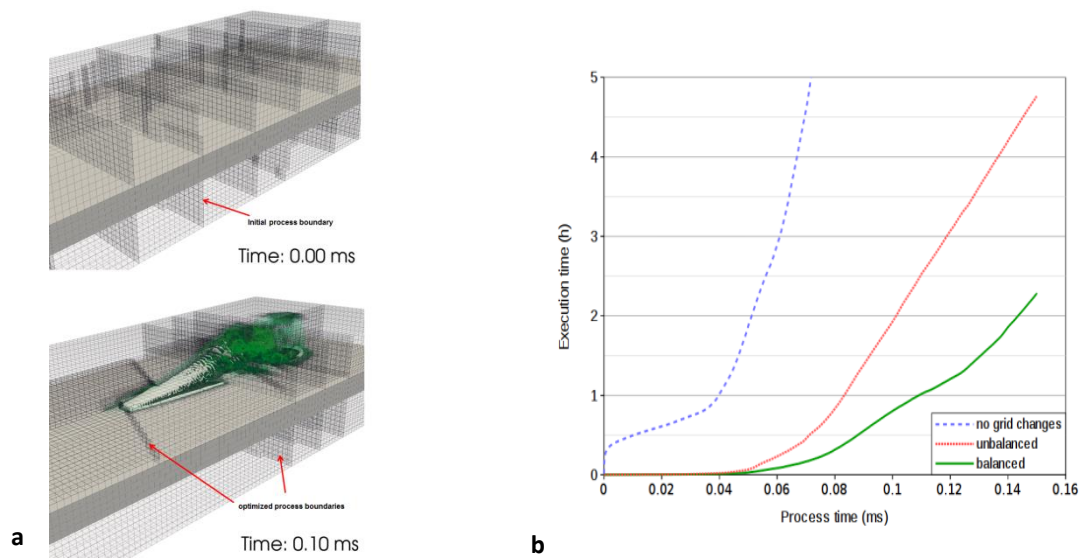

Fig. 11. (a) Above: Initial simulation domain showing the process boundaries. Below: Refined grid with balanced process distribution at a certain time during the simulation. Note that processor boundaries moved towards the refined regions as expected in order to compensate the originated imbalance. (b) Execution time in hours for each of the three simulations. The time saving increase continuously over the course of the simulation. Though not fitting in the plot scale, the total execution time for the case with fixed mesh was slightly higher than 24 hours.

4. Summary and outlook

In this work we showed an overview of the current work of our group concerning the simulation and analysis of laser assisted processes. Key for the excellent agreement with experiments as well as for the meaningful output is the broad-purpose multiphysical simulation model used. Current applications involve welding, cutting, ablation cutting, joining of dissimilar materials, scribing, drilling, coating removal, ultra-short pulse ablation and additive manufacturing, but it is not necessarily limited to the ones mentioned. By improving the capabilities in terms of the physics involved as well as in the overall performance will approach in the forthcoming the analysis of more sophisticated problems.

Acknowledgements

The authors would like to show their gratitude to their cooperation partners from the Laserinstitut Hochschule Mitweida and from the Ernst-Abe-University of Applied Science, as well as to the center for high-performance computation Vienna Scientific Cluster for the support provided in the course of this work.

References

[1] Otto et al.: “Numerical Simulations - A Versatile Approach for Better Understanding Dynamics in Laser Material Processing”, Physics Procedia A, 12, 11-20 (2011) http://dx.doi.org/10.1016/j.phpro.2011.03.003

[2] Tatra et al.: “Numerical Simulation of Laser Ablation with Short and Ultra-short Pulses for Metals and Semiconductors”, Physics Procedia, 83, 1339-1346 (2016) https://doi.org/10.1016/j.phpro.2016.08.141

[3] Voller et al.: “An enthalpy method for convection/diffusion phase change”, International Journal for Numerical Methods in Engineering, 24 (1), 271-284 (1987) http://dx.doi.org/10.1002/nme.1620240119

[4] Otto et al.: “Multiphysical Simulation of ns-Laser Ablation of Multi-material LED-structures”, Physics Procedia, 56, 1315-1324 https://doi.org/10.1016/j.phpro.2014.08.057

[5] Otto et al.: “Simulationsgestützte Analyse des Übergangs zwischen Laser-strahlschweißen und -abtragsschneiden”, Journal of the University of Applied Sciences Mittweida, 4, 56-59 (2015)

[6] Otto et al.: “Numerical and Experimental Investigations of Humping Phenomena in Laser Micro Welding”, Physics Procedia, 83, 1415-1423 (2016) https://doi.org/10.1016/j.phpro.2016.09.004